GNSS TEC-Based Earthquake Ionospheric Perturbation Detection Using a Novel Deep Learning Framework

Pan Xiong, Cheng Long, *Senior Member, IEEE*, Huiyu Zhou, Xuemin Zhang, and Xuhui Shen

***Abstract*—In this article, a new method for seismic ionospheric Global Navigation Satellite System (GNSS) total electron content (TEC) based anomaly detection using a deep learning framework is proposed. The performance of the proposed encoder–decoder long short-term memory extended model is compared with those of five other benchmarking predictors. The proposed model achieves the best performance ($R^2 = 0.9105$ and root-mean-square error (RMSE) $= 2.6759$) in predicting TEC time series data, demonstrating a 20% improvement in R^2 and 39.1% improvement in the RMSE over the autoregressive integrated moving average model. To detect the pre-earthquake ionospheric disturbances more accurately, a reasonable strategy for determining anomaly limits is also proposed. Finally, the method is applied to analyze the pre-earthquake ionospheric TEC disturbance of the 2016 Xinjiang M_s 6.2 earthquake. By excluding the effects of solar activity and geomagnetic activity, obvious ionospheric anomalies could be observed, occurring during 4–8 days prior to, and on 1 day before, the earthquake. Negative anomalies tended to occur in the earlier period, whereas positive anomalies occurred closer to the earthquake time, with increasing anomaly intensity with temporal proximity. Furthermore, confusion analysis is used in this article to verify the reliability of the proposed model. The proposed model achieves significant improvements in predicting GNSS TEC time series and is shown to advance the performance of earthquake anomaly detection technology.**

***Index Terms*—Anomaly detection, deep learning, earthquake, ionospheric perturbation, time series prediction.**

I. Introduction

IT HAS long been recognized that electromagnetic anomalies in the ultralow frequency, extremely low frequency, and very low frequency bands can be detected by ground- and space-based measurements before major earthquakes [1], [2]. Such anomalies may be in the form of signals caused by earthquakes that propagate through the ionosphere and trigger variations in the critical frequency of the F2 layer (values denoted as foF2) and total electron content (TEC) [3]. For instance, research has shown that ultralow-frequency magnetic noise was observed before the M_s (surface wave magnitude) 7.1 Guam earthquake [4]. Similarly, Liu *et al.* reported foF2 and TEC decreases a few days prior to the 1999 M_w (moment magnitude) 7.7 Chi-Chi earthquake [5] and the M_s 9.3 Sumatra–Andaman earthquake on December 26, 2004 [6]. In other examples of noted ionospheric disturbance, Pulinets reported a TEC decrease on the day before the M_s 6.6 San Simeon earthquake [3] and on May 9, three days before the 2008 Wenchuan M_s 8.0 earthquake, TEC inversed by global positioning system (GPS) observations and foF2 from ionosounding were found to have increased significantly [7]–[11]. From further research, significant TEC variations that occurred 20–40 min preceding three recent large earthquakes in Chile (the 2010 Maule M_w 8.8, 2014 Iquique M_w 8.2, and 2015 Illapel M_w 8.3 earthquakes) have also been reported [12]. Multiple other studies showed that clear precursory positive TEC anomalies in the focal region of the 2011 Tohoku-Oki earthquake were detected ~40 min before the earthquake [13]–[15]. Finally, from ionospheric and atmospheric precursory analysis related to three $M_w > 6.0$ earthquakes in Japan, Shah *et al.* [16] found evidence of TEC and foF2 anomalies from 10:00 to 12:00 UT on the day of the main earthquake.

In addition to these seismic case-based studies, seismologists have also extensively conducted statistics-based studies on TEC anomalies prior to large earthquakes. In such research, Chen *et al.* [17] analyzed the TEC of the global ionospheric map using singular spectrum analysis to establish reliable background variability and determine the root-mean-square error (RMSE) of detected anomalies prior to $M_s \geq 6.0$ earthquakes in mainland China from 1998 to 2013. They found that the anomalies were concentrated 1–5 days before the earthquakes and that the anomalies were most obvious near the epicenter. In similar research, Zhu and Jiang [18] statistically investigated ionospheric TEC variations 15 days before and after 276 individual inland earthquakes of $M_s \geq 6.0$. After excluding the disturbance of geomagnetic activity, they found differences in terms of spatial distribution, with the largest differences being in the epicentral

Manuscript received August 15, 2021; revised December 30, 2021 and April 4, 2022; accepted May 11, 2022. Date of publication May 20, 2022; date of current version June 2, 2022. This work was supported in part by the Special Fund of the Institute of Earthquake Forecasting, China Earthquake Administration under Grant 2020IEF0510, Grant 2021IEF0708, and Grant 2021IEF0706; in part by the National Key R&D Program of China under Grant 2018YFC1503505; and in part by the National Natural Science Foundation of China under Grant 41674156. *(Corresponding author: Xuhui Shen.)*

Pan Xiong and Xuemin Zhang are with the Institute of Earthquake Forecasting, China Earthquake Administration, Beijing 100036, China (e-mail: xiongpan@ief.ac.cn; zxm@ief.ac.cn).

Cheng Long is with the School of Computer Science and Engineering, Nanyang Technological University, Singapore 639798 (e-mail: c.long@ntu.edu.sg).

Huiyu Zhou is with the School of Computing and Mathematical Sciences, University of Leicester, LE1 7RH Leicester, U.K. (e-mail: hz143@leicester.ac.uk).

Xuhui Shen is with the National Institute of Natural Hazards, Ministry of Emergency Management of China, Beijing 100085, China (e-mail: shenxh@seis.ac.cn).

Digital Object Identifier 10.1109/JSTARS.2022.3175961

region, whereas the incidence of ionospheric TEC disturbances in the five days before each earthquake was generally higher than that after the earthquake, and both increased slightly with the magnitude. In a comparative study across multiple latitudes, Shah *et al.* [19] studied ionospheric TEC anomalies before and after 1182 $M_w > 5.0$ earthquakes in three different latitude zones from 1998 to 2019. The analysis showed that before earthquakes of $M_w \geq 6.0$ with focal depths of < 220 km (the latitude zone of 25 °N–25 °S), the probability of TEC abnormality was ∼80%. Before earthquakes of $M_w \geq 7.0$ with focal depths of < 120 km (the latitude zones of 80 °N–25 °N and 25 °N–25 °S), the probability of TEC abnormality was 65%. From the perspective of quartiles, Liu *et al.* [20] used the 15-day median value of TEC and the associated interquartile range (IQR) as a reference to determine anomalous signals within TEC data. In the data from the 20 earthquakes of $M_s \geq 6.0$ that occurred in Taiwan from September 1999 to December 2002, preseismic ionospheric anomalies were found between 18:00 and 22:00, in the five days prior to 16 of the 20 cases. Following that study, Liu *et al.* [9] used the same method to count TEC anomalies associated with 35 $M_s \geq 6.0$ earthquakes in China from May 1998 to April 2008. Statistics showed that GPS TEC above the epicenter tended to decrease significantly 3–5 days before the 17 $M_s \geq 6.3$ earthquakes.

These studies show that TEC variations before major earthquakes may be valuable for earthquake prediction, and thus understanding such variations aids the comprehension of earthquake processes. However, these studies mainly focused on statistical analysis based on a selected window of observations. This represents a limitation, as no statistical method can fully learn from previous observations and patterns. In contrast, by using smaller window sizes to learn trends, seasonality, and residual patterns in the data, machine intelligence-based algorithms offer more powerful and robust tools for predicting future observations and improving uncertainty components.

In recent years, statistical model and sophisticated machine intelligence-based methods have been applied to TEC time series for earthquake anomaly detection, including the seasonal autoregressive integrated moving average (ARIMA) [21], [22], deep neural network (DNN) [23], [24], random forest (RF) [25], support vector machine (SVM) [26], and decision tree (DT) [25] methods.

On the other hand, recent research [27], [28] showed that claimed TEC anomalies were actually artifacts. However, their negative response is mainly based on the criticisms to some previous papers [29], [30]. In this article, we do not define anomalies in the same way the criticized papers define the TEC anomalies.

In general, machine intelligence-based methods operate by predicting the signal at any given point and testing whether the difference between the true value and the predicted value is sufficient to treat it as an anomaly. This approach allows the visualization of confidence intervals, which help validate the occurrence of anomalies and explain why they occur. In this study, we combine this idea with a novel encoder–decoder (ED) long short-term memory extended (LSTME, or collectively ED-LSTME) neural network [31] to show that it is possible to detect TEC anomalies associated with earthquakes. For this purpose, we collected Global Navigation Satellite System (GNSS) TEC data from the Crustal Movement Observation Network of China (CMONOC). TEC data from 2012 to 2015 were used to build and train the ED-LSTME model, and data of the Xinjiang M_s 6.2 earthquake (December 8, 2016) were assessed as a case study. The ED-LSTME model experiment was designed such that TEC values were predicted for four weeks before and one week after the earthquake in order to detect TEC anomalies by comparing the predicted and true values. We also compared the prediction performance of the ED-LSTME model with the ARIMA, DNN, RF, SVM, and DT models, and compared the seismic anomaly detection results of the ED-LSTME model with the classic IQR method [20].

II. Data and Methodology

A. Data and Data Preprocessing

The CMONOC GNSS data used in this study were obtained from 260 stations covering mainland China. The GNSS data of CMONOC are available on the SHAO platform (SHA[1]) for GNSS data analysis. The M_s 6.2 Xinjiang earthquake occurred in Hutubi County, Changji Prefecture, Xinjiang; the epicenter was located at 43.83 °N and 86.35 °E at a depth of 6.0 km. The earthquake occurred at 13:15 on December 8, 2016. The five GNSS stations closest to the earthquake (XJSH, XJWL, XJDS, XJKE, and XJXY) were selected for the study. Fig. 1 shows the spatial distribution of the five GNSS stations; the detailed geographical locations are listed in Table I.

This research involved two phases. The first phase was to construct and train the ED-LSTME model for the selected five GNSS stations. The ED-LSTME model consisted of the following three inputs.

1) Vertical TEC values with a temporal resolution of 15 min.
2) The K_p index, which was exploited to respond to solar particle radiation, wherein the solar radio flux of 10.7 cm (2800 MHz; F10.7 index) was used as an indicator of solar activity.
3) The geomagnetic index a_p, which was used as an indicator of overall geomagnetic activity and magnetic storms.

We used a well-established technique for the vertical TEC derivation, detailed descriptions of which are given by Choi *et al.* [32] and Xiong *et al.* [31]. We used GNSS TEC data from 2002 to 2004 as the training dataset and data from 2005 as the test dataset. The second phase was the use of the trained ED-LSTME model to predict TEC data 28 days before and 7 days after the 2016 M_s 6.2 Xinjiang earthquake (i.e., from November 17 to December 14, 2016), and to obtain TEC anomalies by calculating the upper (UB) and lower (LB) bounds of the predicted and true values.

We calculated the mean and standard deviation of the TEC time series for each station and then calculated appropriate thresholds to identify and exclude outliers, outliers were considered as values that were more than three standard deviations from the mean. Moreover, we chose Kalman smoothing [33] to fill in the removed and missing data.

[1][Online]. Available: http://www.shao.ac.cn/shao_gnss_ac

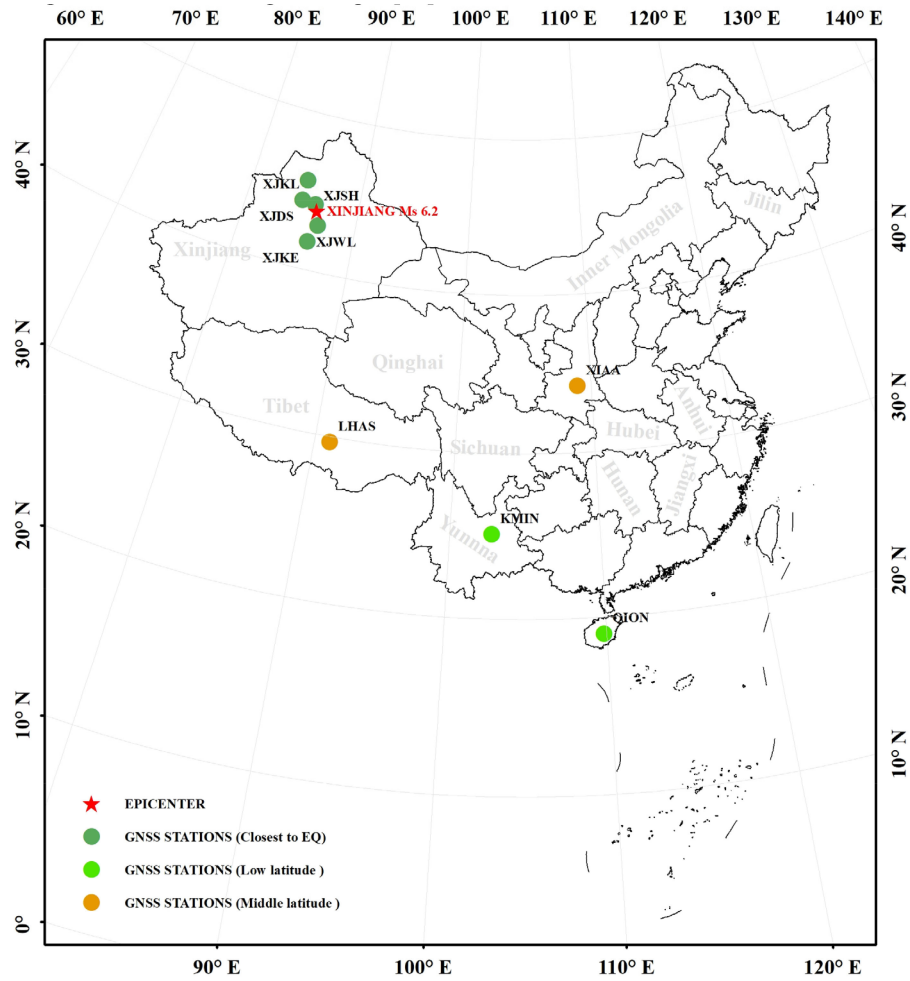

Fig. 1. Study region and spatial distribution of GNSS stations.

TABLE I
GNSS STATIONS

Station code	Station name	Province	Geographic Latitude	Geographic Longitude	Distance to Epicenter	Geomagnetic Latitude	Geomagnetic Longitude
XJSH	Shizihe	Xijiang	44.2°E	86.1°N	45.73 km	35.16°N	161.43°E
XJWL	Wulasitai	Xijiang	42.9°E	86.7°N	107.21 km	33.83°N	161.85°E
XJDS	Dushanzi	Xijiang	44.3°E	84.8°N	134.41 km	35.32°N	160.30°E
XJKE	Kuerlei	Xijiang	41.7°E	86.1°N	237.71 km	32.66°N	161.22°E
XJKL	Kelamayi	Xijiang	45.6°E	84.9°N	227.71 km	36.62°N	160.51°E
XIAA	Xi'an	Shanxi	34.180°N	108.990°E		24.60°N	178.48°W
LHAS	Lhasa	Tibet	29.660°N	91.100°E		20.43°N	164.96°E
KMIN	Kunming	Yunnan	25.030°N	KMIN		15.50°N	175.75°E
QION	Qiongzhong	Hainan	19.030°N	QION		9.51°N	177.57°W

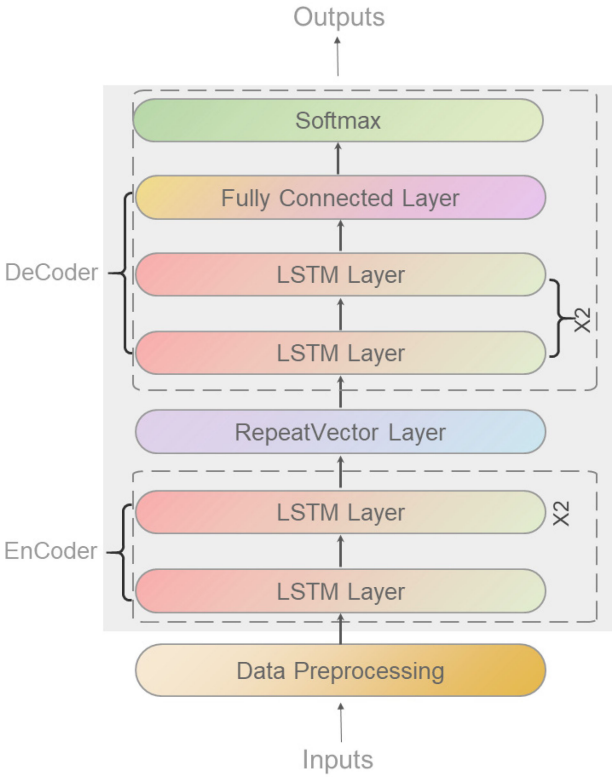

Fig. 2. Network framework of the ED-LSTME model.

Sample modeling is an important step in time series data preprocessing that can transform data to an input for machine learning or deep learning models. In this study, the sliding window was used as a representative modeling technique [34], which is designed to check the predictive power of several sequential models. The implementation steps are described in detail by Xiong *et al.* [31].

B. TEC Anomaly Detection Using the ED-LSTME Model

1) Forecasting TEC Time Series With the ED-LSTME Model: As shown in Fig. 2, the ED-LSTME model is used to map input and output sequences of arbitrary length [35]. Encoder components can be obtained by applying one or more long short-term memory (LSTM) layers. The model output is a fixed-size vector, which is defined by the number of memory units in this layer. Decoder components can also be implemented using one or more LSTM layers and by converting the internal representation into the correct output sequence. Representative features were extracted from historical TEC data and auxiliary input data (a_p index, the K_p index, and F10.7 index) through the LSTM layer. Specifically, time-delayed TEC historical data and current auxiliary data of the solar flux index K_p and geomagnetic activity index a_p from all selected GPS stations were concatenated and stacked to compose an input sequence for the LSTM layers. The RepeatVector layer [36] was used as the adapter for the network encoding and decoding part. For a detailed description of the model, please refer to the work by Xiong *et al.* [31]. The hyperparameters used in the ED-LSTME model in this study were the same as the parameters in the trained model of Xiong *et al.* [31].

2) TEC Anomaly Detection: After obtaining the predicted values using the ED-LSTME model, the rolling mean and rolling standard deviation of the difference between true and predicted values were computed for TEC anomaly detection, which involved the following three steps.

1) Calculate the error term (i.e., the difference between true and predicted values).
2) Select the number of consecutive observations per rolling window (the size of the rolling window), and calculate the rolling mean (μ) and rolling standard deviation (σ); the window size was 15 days in this study.
3) Classify data with an error of two standard deviations as the limit for anomalies. The LB and UB are defined by (1) and (2), respectively

$$\text{Lower Bound} = \mu - 2\sigma \tag{1}$$

$$\text{Upper Bound} = \mu + 2\sigma. \tag{2}$$

Observed TECs exceeding the UB and LB were regarded as positive and negative anomalies, respectively.

C. Comparison of Methods

To assess the performance of the proposed model for time series forecasting, the ED-LSTME model was compared with other algorithms for TEC anomaly detection (DNN [37], RF [38], SVM [39], DT [40], and ARIMA [41]), all of which have exhibited good performance in past studies [21], [23], [25], [26], [42], [43]. As the investigated models are sensitive to parameter selection, we chose parameters that yielded the best performance using hyperparameter tuning.

To evaluate the performance of these algorithms, we implemented four different statistical indicators, including RMSE, the coefficient of determination (R^2), mean absolute error (MAE), and the correlation coefficient (ρ), calculated as follows:

$$\text{RMSE} = \sqrt{\frac{1}{n}\sum_{i=1}^{n}\left(y_i - y_i^*\right)^2} \tag{3}$$

$$R^2 = \left(\frac{\sum_{i=1}^{n}\left(y_i - \overline{y}\right)\left(y_i^* - \overline{y^*}\right)}{\sqrt{\sum_{i=1}^{n}\left(y_i - \overline{y}\right)^2}\sqrt{\sum_{i=1}^{n}\left(y_i^* - \overline{y^*}\right)^2}}\right)^2 \tag{4}$$

$$\text{MAE} = \frac{1}{n}\sum_{i=1}^{n}\left|y_i - y_i^*\right| \tag{5}$$

$$\rho = \frac{\sum_{i=1}^{n}\left(y_i^* - \overline{y^*}\right)\left(y_i - \overline{y}\right)}{\sqrt{\sum_{i=1}^{n}\left(y_i^* - \overline{y^*}\right)^2}\sum_{i=1}^{n}\left(y_i - \overline{y}\right)^2} \tag{6}$$

where n is the number of cases; y_i is the observed value of the ith case; y_i^* is the predicted value; and $\overline{y}$ and $\overline{y^*}$ are the mean values of y_i and y_i^*, respectively.

TABLE II
PREDICTION ACCURACIES OF SIX MODELS FOR ALL GNSS STATIONS

Model	Metric	All Stations	XJSH	XJWL	XJDS	XJKE	XJKL
ED-LSTME	R^2	0.9105	0.9045	0.9103	0.9467	0.8806	0.9483
	MAE	1.7438	1.5404	1.5188	1.376	2.4354	1.539
	RMSE	2.6759	2.4641	2.3929	2.0657	3.3834	2.2116
	ρ	0.9552	0.9513	0.9545	0.9731	0.9543	0.9745
DNN	R^2	0.8898	0.8965	0.9021	0.9445	0.8786	0.9455
	MAE	1.8788	1.567	1.5241	1.3918	2.2737	1.5226
	RMSE	2.9697	2.5661	2.5006	2.1088	3.4112	2.2706
	ρ	0.9436	0.9469	0.9499	0.9721	0.9396	0.9727
RF	R^2	0.881	0.8884	0.8959	0.9386	0.7755	0.9423
	MAE	1.8846	1.6278	1.5931	1.503	3.265	1.6125
	RMSE	3.0865	2.6636	2.5784	2.2181	4.6394	2.3358
	ρ	0.9387	0.9436	0.9476	0.9698	0.8868	0.9721
SVM	R^2	0.8725	0.8869	0.8932	0.9344	0.7548	0.9422
	MAE	2.0791	1.6834	1.6542	1.5688	3.0866	1.6618
	RMSE	3.1945	2.6821	2.6119	2.2935	4.8491	2.3383
	ρ	0.9409	0.9431	0.9462	0.9699	0.8692	0.9713
ARIMA	R^2	0.7586	0.8292	0.8175	0.8949	0.216	0.9086
	MAE	1.785	1.8372	2.0012	2.09	2.9512	2.0315
	RMSE	4.3948	3.2955	3.4135	2.9022	8.6702	2.9395
	ρ	0.8804	0.9157	0.9135	0.9491	0.6811	0.9597
DT	R^2	0.6838	0.7858	0.7974	0.872	0.1912	0.8715
	MAE	2.6291	2.2961	2.2534	2.1601	4.0577	2.3783
	RMSE	5.0302	3.6904	3.5965	3.2032	8.8059	3.4865
	ρ	0.8502	0.8933	0.8984	0.9357	0.6767	0.9354

To compare the performance of the ED-LSTME model in detecting TEC anomalies before and after earthquakes, we applied the IQR method, a classic anomaly detection method in seismic ionospheric studies [5], [44] wherein TEC time series are modeled by the mean (M) or median ($\tilde{M}$), and anomalies are defined by the standard deviation (σ) or IQR. In our approach, the median ($\tilde{M}$) at the corresponding time of the first 15 days was taken as the background value, and the UB and LB of its IQR were calculated. Here, IQR $= 1.34\sigma$, that is, the expected value of the quartiles is 1.34 times that of the standard deviation, to find the difference from the TEC observed on the 16th day. The LB and UB are defined as follows:

$$\text{LB} = \tilde{M} - 1.5IQR \tag{7}$$

$$\text{UB} = \tilde{M} + 1.5IQR. \tag{8}$$

The space weather (K_p) and disturbance storm-time (Dst) indices were also used as references to determine if the TEC anomalies were related to the effects of space weather. The threshold values $K_p < 3$ and Dst > -30 nT indicate relatively quiet solar and magnetic ionospheric activity, respectively.

III. RESULTS AND DISCUSSION

A. Model Performance Comparison for Time Series Forecasting

The performance of the various models over all stations is detailed in Table II. The R^2 and RMSE values varied from 0.6838 to 0.9105 and 2.6759 to 5.0302 TEC units, or TECU, respectively. The performance of the simplest ensemble machine learning method (DT) was the worst, but RF, which combines a set of binary DTs, delivered better performance (28.8% improvement in R^2 and 38.6% reduction in RMSE over the DT model). The ARIMA model, which is a traditional time-series forecasting method, also performed poorly ($R^2 = 0.7586$, RMSE $= 4.3948$). An improved R^2 value (0.7586–0.8725) was obtained for the SVM model, indicating that separating the hyperplane with the largest geometric interval delivered better performance.

As the DNN model can deal with scenarios that include multiple input variables using multiple fully connected layers, it delivered a slight improvement compared with RF and SVM, with an increase of 0.01 for R^2 and a decrease of 0.23 TECU for RMSE. As an intelligent algorithm, the ED-LSTME model achieved the best performance ($R^2 = 0.9105$ and RMSE $=$ 2.6759) among all considered models.

In addition, to visually demonstrate the forecasting performance of each model, scatter plots of the cross-validation results were used to show predictions and actual values. Fig. 3 provides a visual performance comparison of the considered models; the ED-LSTME model shows a strong, positive, and linear association between estimated and observed TECs, with few outliers in the data. Looking at the other models, although their form is also linear, the association appears to moderate, and there are more outliers.

The effectiveness of the ED-LSTME model was further evaluated using Taylor diagrams [45]. The ED-LSTME model performed significantly better than other models, with a stronger

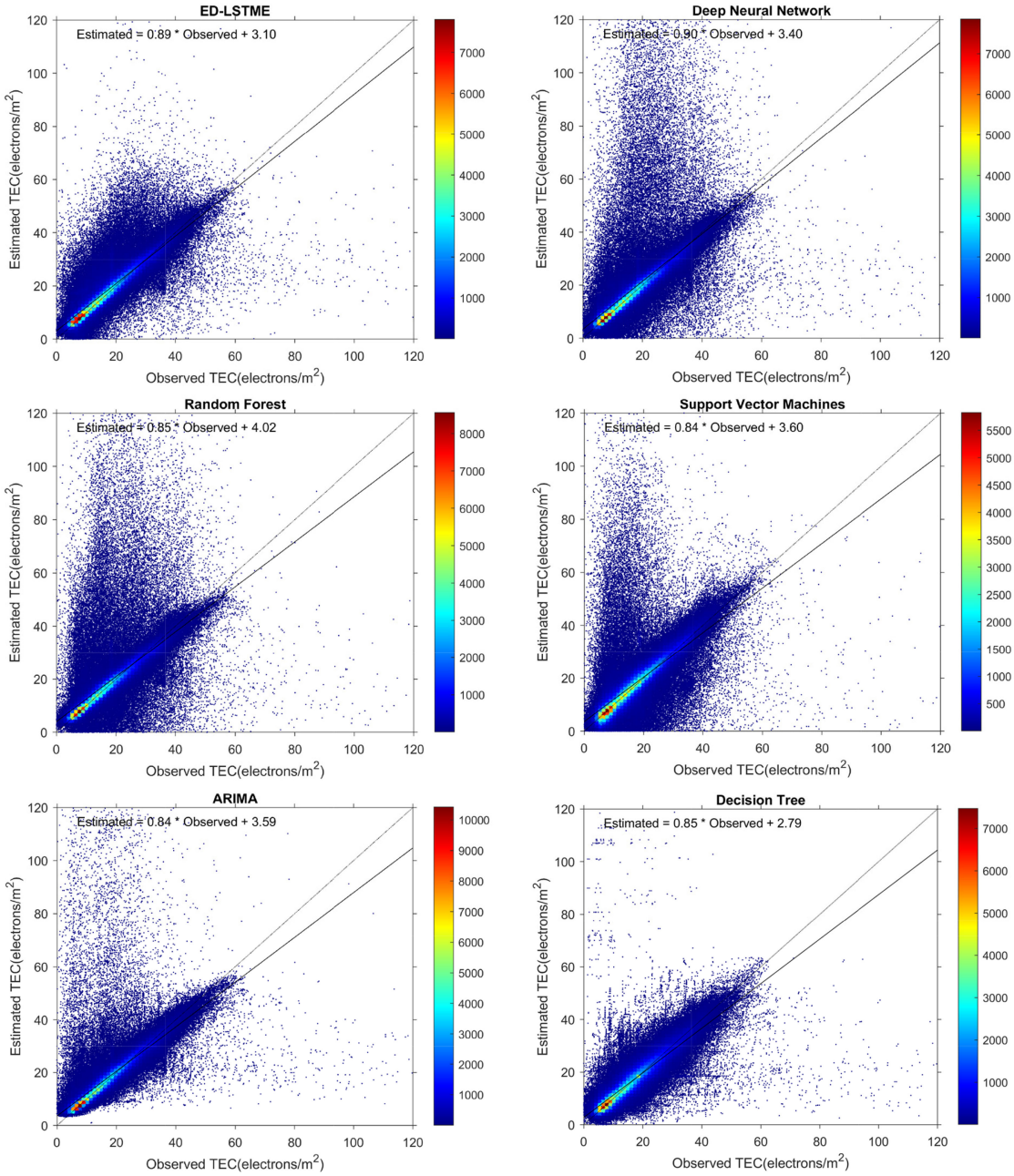

Fig. 3. Prediction results of the ED-LSTME, DNN, RF, SVM, DT, and ARIMA models.

correlation to the expected results and a lower standard deviation in comparison (see Fig. 4). The R^2 ranges of the other models were from 0.85 to 0.95 and standard deviations were from 8.73 to 11.34. The ED-LSTME model had a higher correlation (by 0.01), and lower standard deviation (by 0.7 TECU) compared with the next-best DNN model. Compared with other methods, the ED-LSTME model displayed very little bias (0.03). Based on these results, the ED-LSTME model significantly outperforms other models.

Bar curves of the four statistical indicators were used to assess the performance of the various models for each TEC station (see Fig. 5 and Table II). The ED-LSTME model had the highest forecasting efficiency at each station. The forecasting performance at the XJKE station was the worst among all stations, especially when using the ARIMA and DT models. A possible explanation is that the magnetic latitude of the XJKE station is the lowest among the five stations, and the influence of the disturbance known as the equatorial ionospheric anomaly at lower latitudes may have resulted in higher RMSEs. To validate this phenomenon, stations at different latitudes were selected to conduct experimental analyses in this article. Specifically, the mid-latitude stations XIAA and LHAS, as well as the low-latitude stations KMIN and QION were used (see Fig. 1 and Table I). Fig. 5 depicts the analysis results, where both different TEC prediction techniques and evaluating metrics show that the prediction performance is greatly influenced by the latitude, and

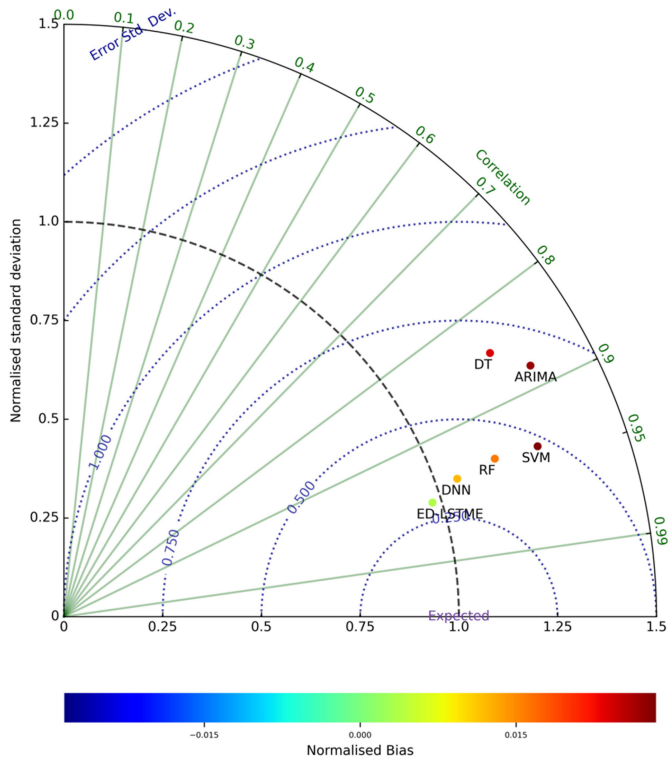

Fig. 4. Taylor diagram of model bias and standard deviation of errors of the ED-LSTME, DNN, RF, SVM, DT, and ARIMA models. The azimuth indicates correlation, the radial distance represents the standard deviation, and the semicircles centered on the "Expected" label represent the error of the standard deviation. The color scale represents the degree of bias.

the prediction performance is relatively low for stations at low latitudes. This result is consistent with statistical results related to ionospheric TEC forecasting [31], [46].

From Fig. 5, we could observe that the prediction accuracy of ED-LSTME and DNN is close when each station is considered individually, whereas if all stations are included under consideration, it is obvious that the prediction performance of ED-LSTME is better than that of DNN. The possible explanation for this is that the amount of data from individual stations is not sufficient, and it is difficult to discriminate the prediction performance. Moreover, a comparison of the prediction errors under disturbed conditions is shown in Fig. 5, where the ED-LSTME model yields the best predictions, probably because the model uses solar and geomagnetic activity values as the input. Under quiet and disturbed conditions, the ED-LSTME model could effectively predict short-term changes in TEC during solar flux and geomagnetic events [31].

B. Anomaly Analysis and Comparison of Earthquake Cases

We used the ED-LSTME model to analyze the ionospheric TEC anomalies of the five GNSS TEC stations closest to the epicenter of the 2016 M_S 6.2 Xinjiang earthquake for a total of 12 days (8 days before and 3 days after the earthquake; Fig. 6).

From Fig. 6, except for the 7th day before the earthquake, the TEC time series of all GNSS stations on the other 9 days and the day of the earthquake had obvious anomalies detected by the ED-LSTME model. Among them, anomalies from the 2nd day before the earthquake (December 6), the day of the earthquake (December 8), and the 3 days after the earthquake (December 9–11) are related to extreme weather in space, that is, it can be confirmed that the anomalies were not caused by the earthquake based on the K_p and Dst indices. Among the anomalies on other days, a mild negative anomaly, which appeared beginning on the 8th day before the earthquake and was strengthened on the 6th and 5th days before the earthquake, changed from a negative to positive anomaly on the 4th day before the earthquake, and then showed a gradual increase until the time of the earthquake.

To validate the anomaly detection results, we performed anomaly detection on the same TEC data based on the IQR method. It can be observed in Fig. 7 that the intensity of the anomalies extracted by the IQR method is significantly weaker than for those detected by the ED-LSTME model. The synchronization anomalies of each station are mainly concentrated on the 2nd day before the earthquake (December 6), the day of the earthquake (December 8), and the 3 days after the earthquake (December 9–11), all of which are days when the anomalies appear to coincide with periods of elevated space activity; in contrast, there are almost no anomalies when space activity is low. Thus, it can be inferred that space activities (e.g., magnetic storms) may contribute to larger disturbances, for which the IQR method is more sensitive. For earthquakes of relatively low magnitudes, the disturbances are not large and may be easily overlooked using the IQR method. In addition, most of the anomalies detected by the IQR method in this study are negative.

Furthermore, a confutation analysis is used in this article to validate the reliability of the proposed ED-LSTME model. Data from March 27 to April 7, 2016 were selected in this article, during this period there were no earthquakes and the space weather was quiet. The results from Fig. 8 demonstrate that the ED-LSTME method does not detect any anomalies, which confirm that the method could avoid false alarms of earthquake anomalies as well as validate its effectiveness in detecting earthquake anomalies.

To verify our conclusions, we observed the earthquake-related anomalies from another perspective. First, we collected outgoing longwave radiation (OLR) data obtained by the NOAA-18 satellite from September 2007 to December 2016. From this datum, OLR anomalies were detected using the robust satellite data analysis (RST) method (see Fig. 9), which utilizes many years of satellite thermal infrared data and is robust for detecting seismic thermal infrared anomalies according to previous studies [47], [48]. The implementation of the RST method is described in detail in a previous study [49]. The main temporal and spatial characteristics of the OLR anomalies can be described as follows (see Fig. 9).

1) From November 30 to December 2, the thermal infrared anomaly was located northeast of the epicenter and showed the characteristics of increasing enhancement degree and expanding area of the enhancement zone.
2) From December 3 to 4, the thermal infrared anomaly developed along the fracture zone to the southwest of the epicenter.

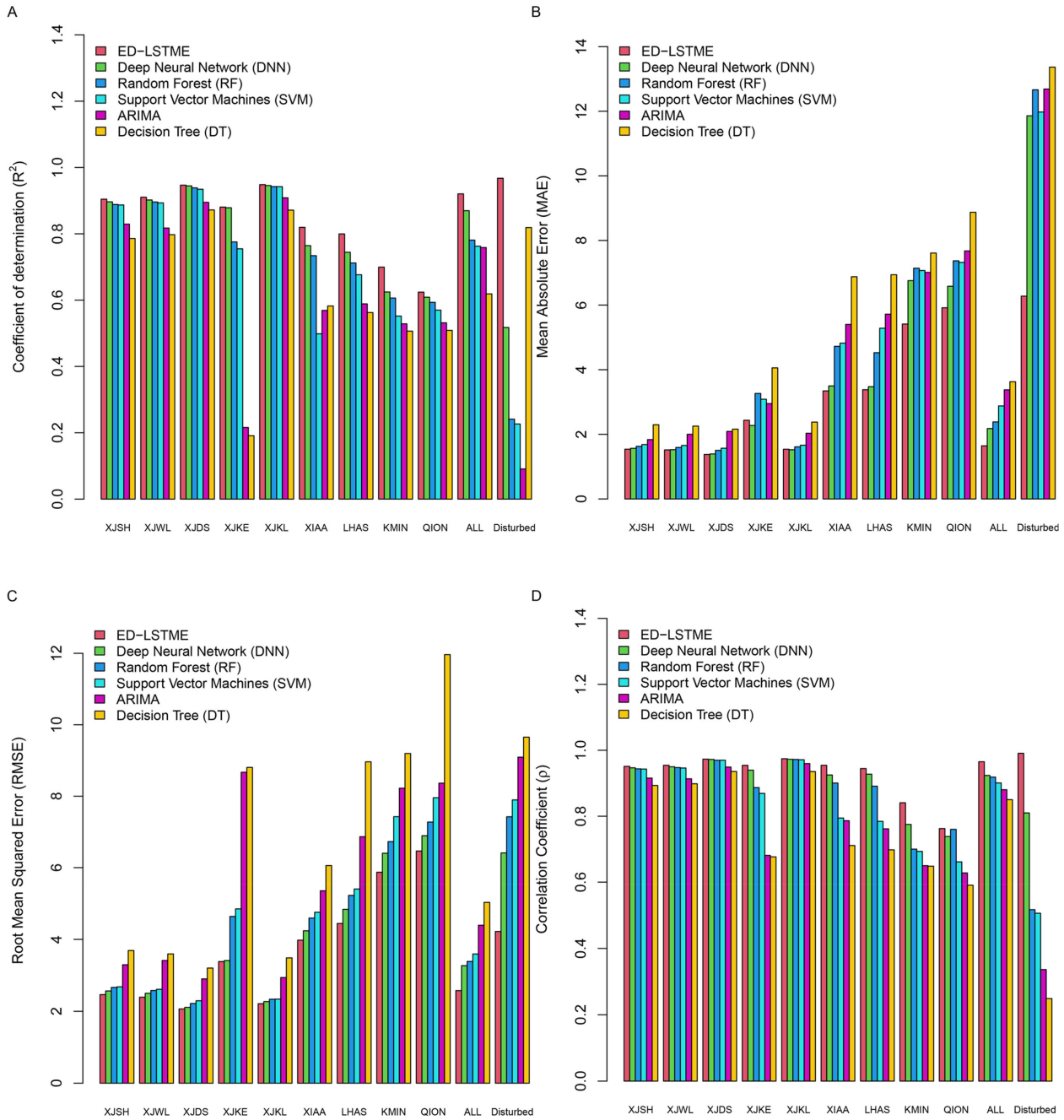

Fig. 5. Bar graph illustrating the (a) coefficient of determination R^2, (b) MAE, (c) RMSE, and (d) correlation coefficient (ρ) between the measured and predicted TEC estimated based on the ED-LSTME, DNN, RF, SVM, DT, and ARIMA models.

3) The period from December 5 to 7 was important for seismic thermal infrared abnormal development, in that, the total area of the isolated anomaly increased sharply and the temperature increased along the fault zone from west to east toward the epicenter, whereas the area and intensity of the anomaly reached its peak on December 7, one day before the earthquake.
4) On December 8, the day of the earthquake, the infrared anomaly faded briefly and the directionality was not obvious. Over the subsequent two days, there was a rapid weakening of the thermal infrared anomaly. Since OLR data are not affected by space weather, the anomalies detected based on OLR data can be considered to be caused by earthquakes.

In previous studies, pre-earthquake TEC anomalies have tended to appear earlier and have a larger impact range; therefore, to further compare the IQR and ED-LSTME methods, data from a longer period of time were selected for processing and analysis. For this purpose, we used TEC data from 3 weeks before to 1 week after the earthquake (November 17 to December 4, 2016) from the five stations closest to the epicenter (see Fig. 10). By visual inspection, it is clear that

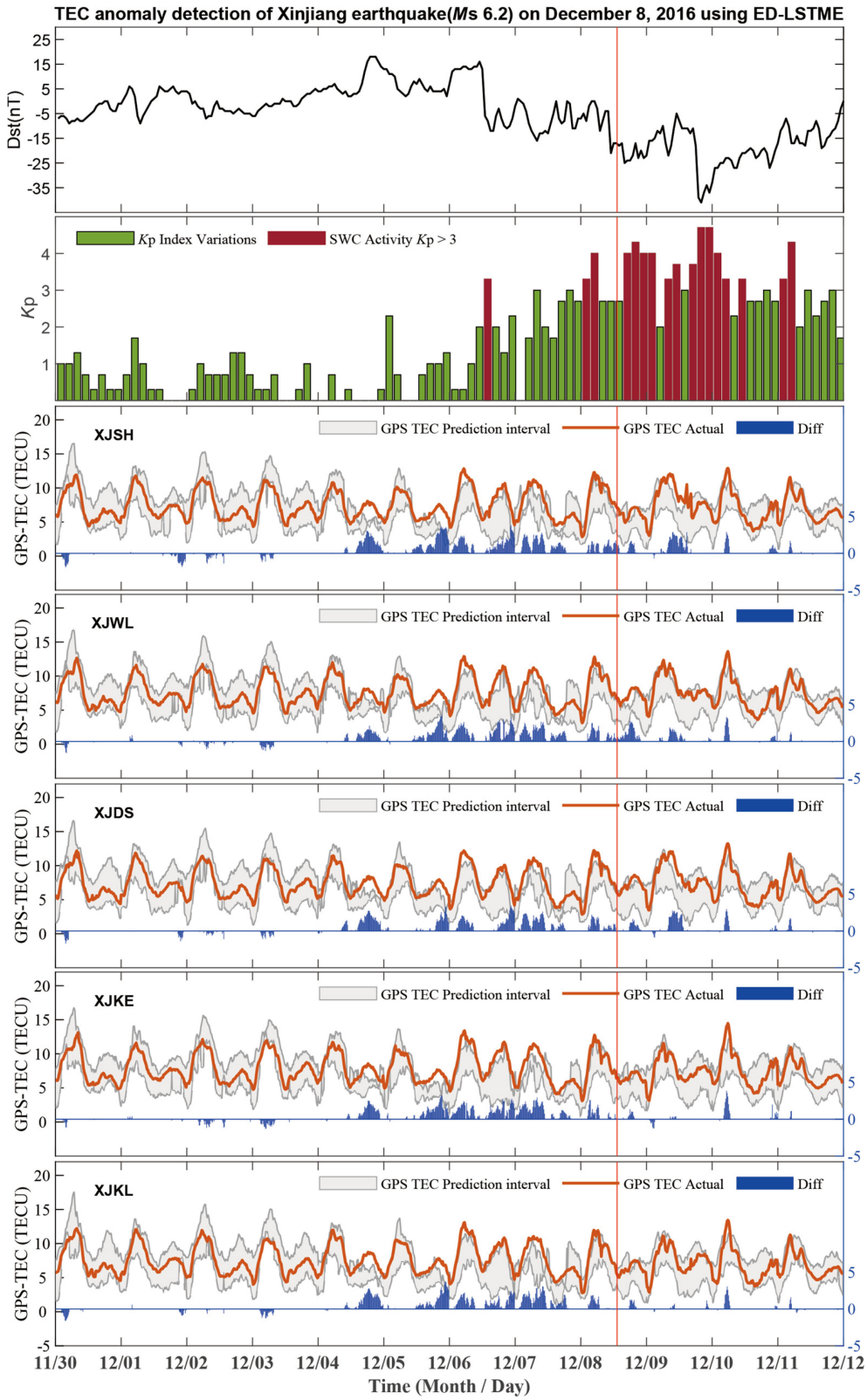

Fig. 6. Anomaly detection of ionospheric TEC variations using the Dst and K_p indices over the five GNSS stations from 8 days before to 3 days after the Xinjiang M_s 6.2 earthquake using the ED-LSTME model.

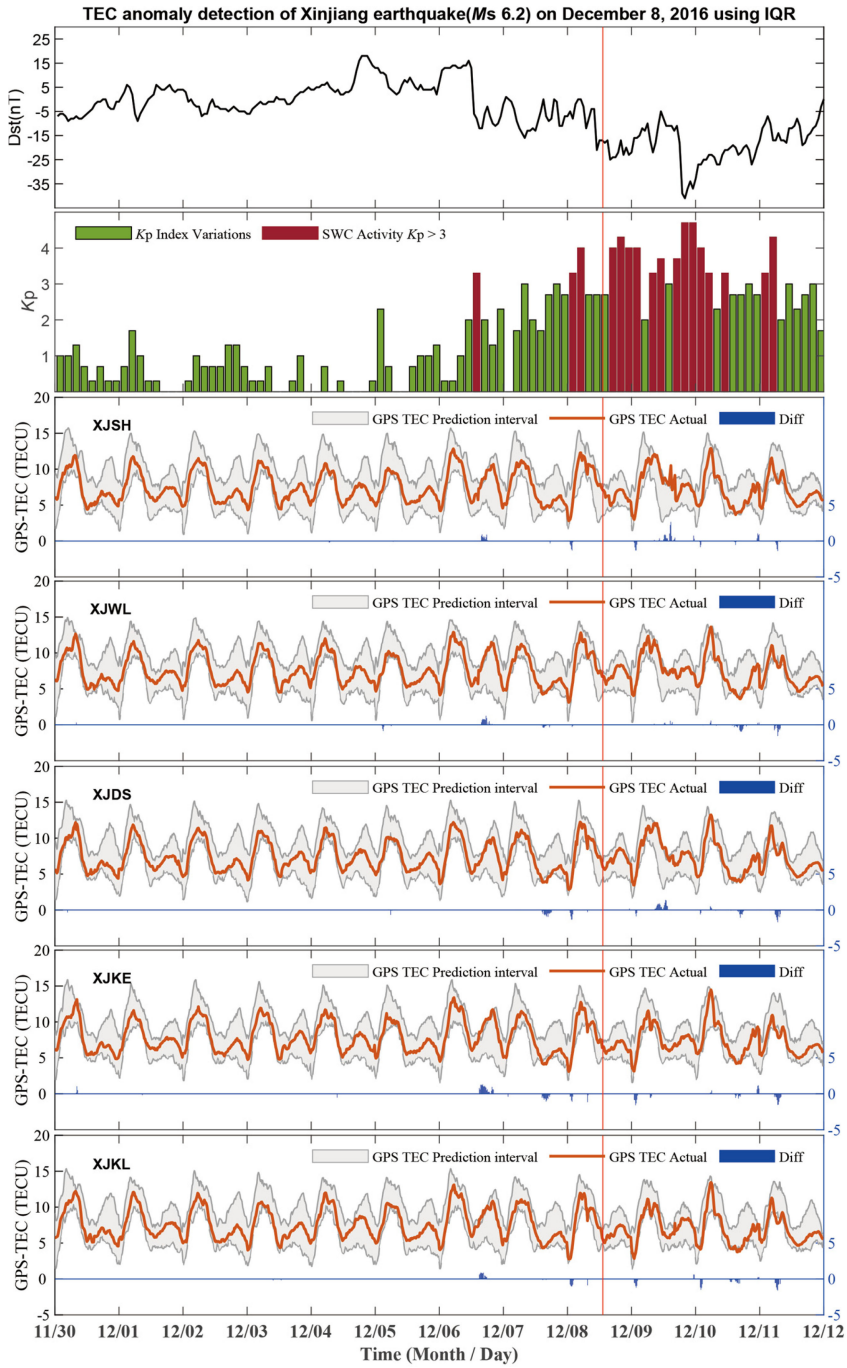

Fig. 7. Anomaly detection of ionospheric TEC variation using the Dst and K_p indices at the five GNSS stations from 8 days before to 3 days after the Xinjiang M_s 6.2 earthquake using the IQR model.

most of the anomalous TEC values occurred around the day of the earthquake, especially between 7 days before and 2 days after.

Fig. 11 illustrates variations in the Dst and K_p geomagnetic indices from November 17 to December 4, 2016. Anomalous Dst values can be observed 13–14 days before and 1–2 days after the earthquake, indicating high geomagnetic activity. The Dst values exceeded the LB value (i.e., −30 nT) at 13:00 on the 14th day before the earthquake, then gradually decreased, reaching a minimum at ∼6:00 on the 13th day before the earthquake. In addition, anomalous values of Dst can be seen 1–2 days after the earthquake. The K_p geomagnetic index in Fig. 11 shows that strong geomagnetic activity (K_p greater than 3.0) occurred 13–16 days before the earthquake and 1–3 days after the earthquake. The K_p values exceeded 4.0 on the 16th day before the earthquake and increased to a maximum value of 5.3 on the 13th before the earthquake. The high K_p values between 13:00 and 15:00 on the 2nd day before the earthquake and on the day of the earthquake can be interpreted to indicate high geomagnetic activity. It can be concluded that such anomalous

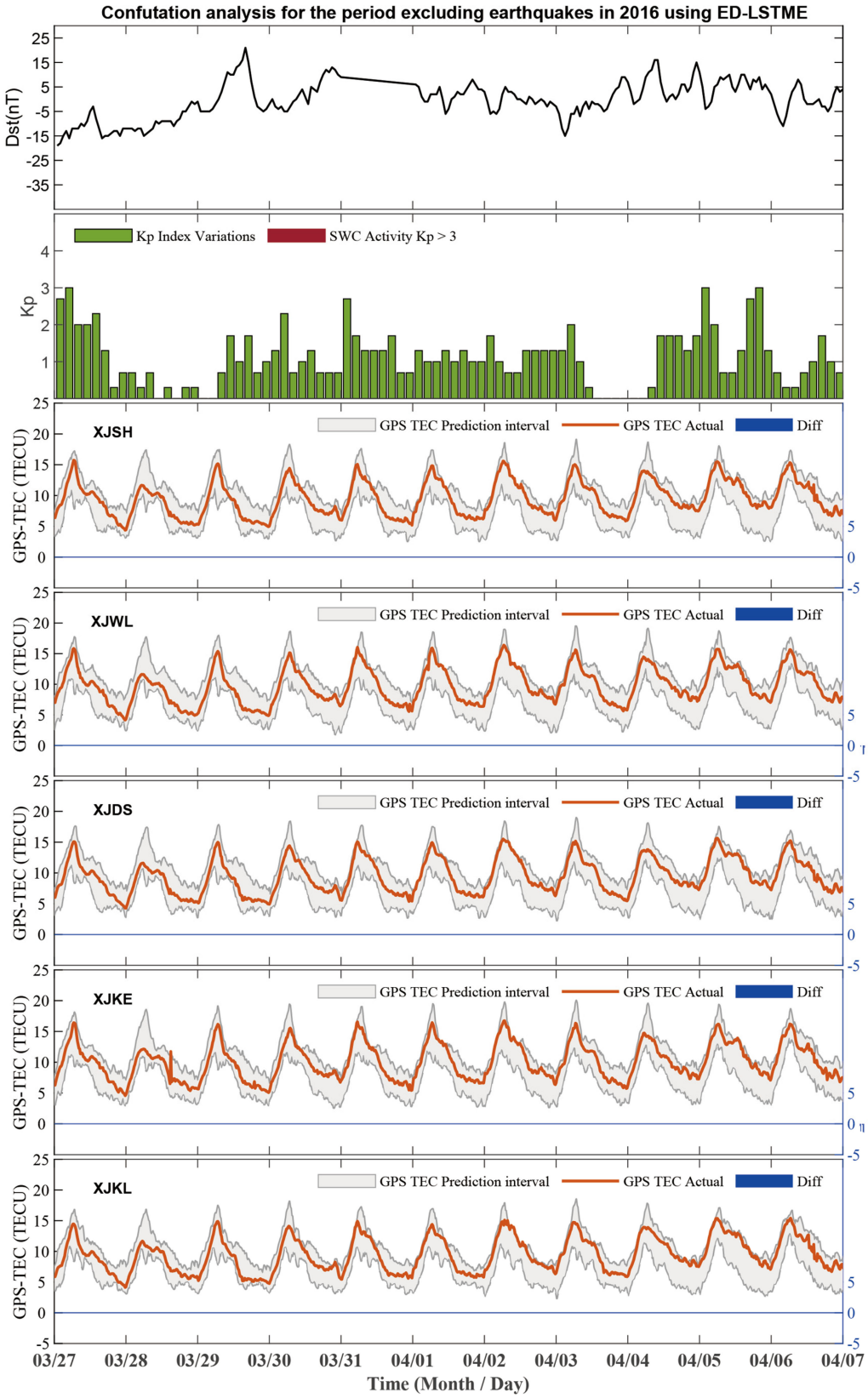

Fig. 8. Confutation analysis for the period excluding earthquakes in 2016 using ED-LSTME.

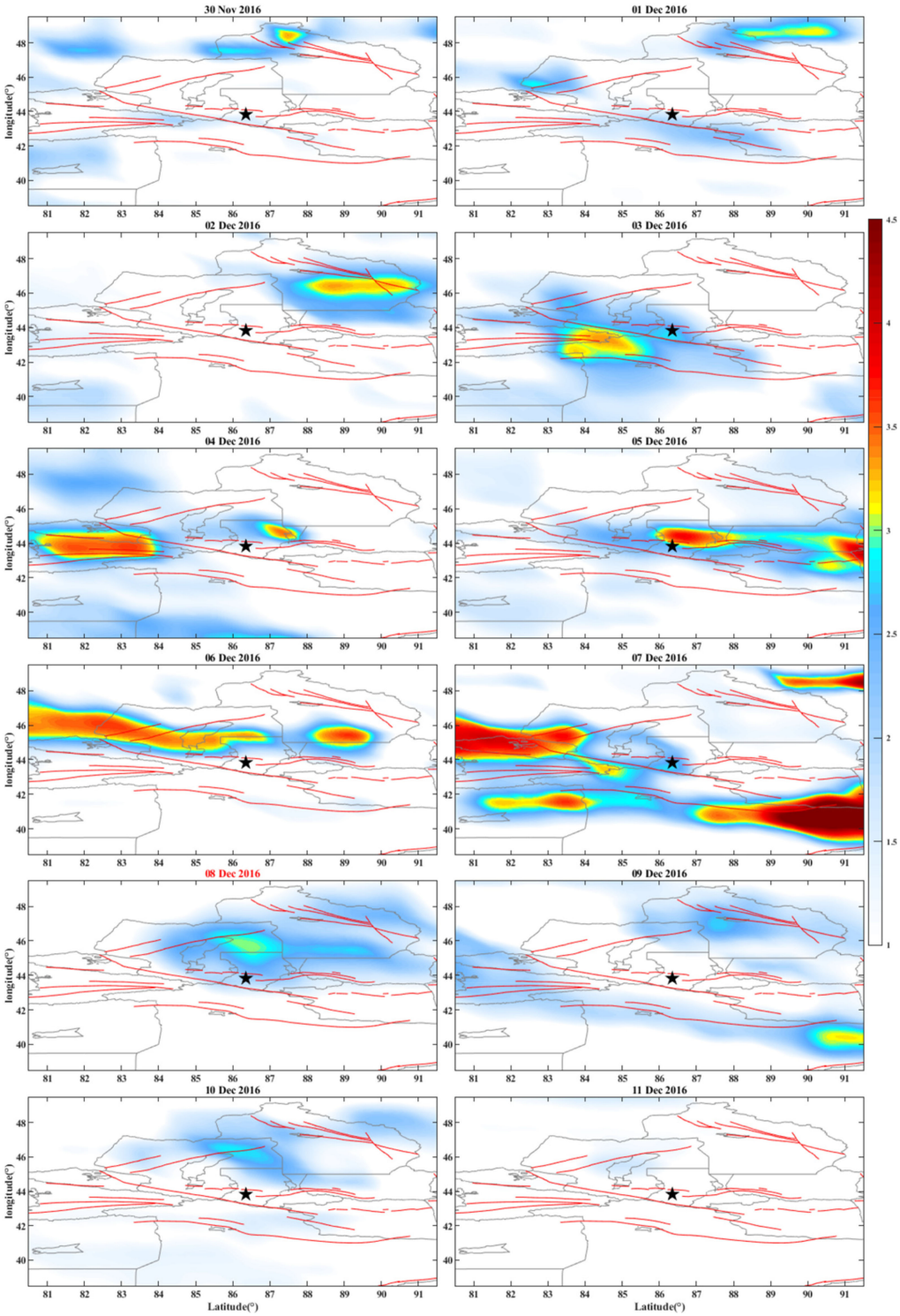

Fig. 9. Daily OLR variation curves from 8 days before to 3 days after the Xinjiang M_s 6.2 earthquake using the RST method. Black stars denote the epicenter, red lines indicate the main active faults, and gray lines denote tectonic plate boundaries.

variations in K_p and Dst may be able to conceal pre-earthquake and postearthquake ionospheric anomalies.

The differences between the actual observed values and predicted value limits (denoted as the "difference in TEC" or DTEC) were extracted separately. Fig. 10 shows variations in DTEC from November 17 to December 4, 2016.

Obvious TEC anomalies occurred from 7 days before the earthquake to 2 days after the earthquake, and the anomaly reached its maximum peak value 1 day before the earthquake. In this study, three conditions ($|\text{DTEC}| > 0.0$, $K_p < 3.0$, and $\text{Dst} > -30$ nt) were used to distinguish between earthquake anomalies and space weather-related anomalies. After excluding

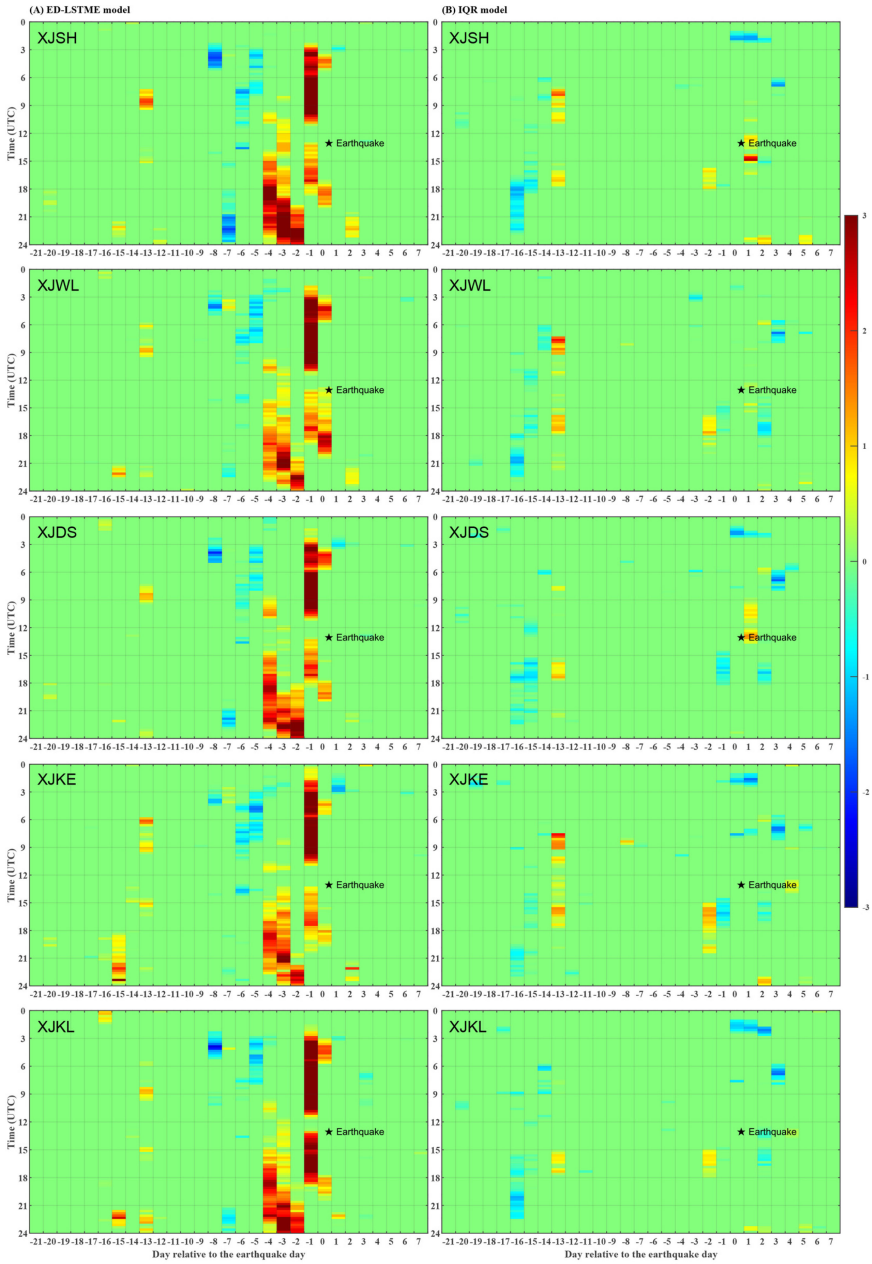

Fig. 10. Comparison of detected TEC anomalies using (a) the ED-LSTME model and (b) the IQR model at five GNSS stations. The *X*-axis represents days relative to the earthquake day and the *Y*-axis represents the universal time coordinate (UTC). The epicenter is marked by a black star.

high geomagnetic activity, the synchronization anomalies of the five stations from 8 to 4 days before the earthquake, and on 1 day before the earthquake, could be regarded as having been caused by the earthquake. The characteristics of the anomalies are as follows: negative anomalies appeared first, then became positive and reached their maximum values 1 day before the earthquake. Anomalies mostly appeared from afternoon to nighttime (15:00–24:00). It can be seen in Fig. 10(a) that certain detected anomalies were masked by high geomagnetic activity. It can be seen in Fig. 10(b) that the IQR method could clearly identify TEC anomalies from 21 days before to 7 days after the earthquake. Relative to Fig. 10(a), the number and intensity of anomalies are substantially reduced; the remaining anomalies appear only on the 4th and 3rd days before the earthquake, whereas the intensity of the anomalies is low and they do not appear at all stations. This confirms our previous conclusion that the IQR method is more sensitive to greater geomagnetic activity and may miss anomalies caused by earthquakes of modest magnitudes.

To summarize, combining the effects of geomagnetic activity and infrared anomalies around the time of the earthquake, the highest deviations from the normal state occurred within 4–8 days and 1 day before the earthquake.

C. Discussion

Our results show that deep learning models (ED-LSTME and DNN models) have better time-series prediction capabilities than other models [50]. This can be explained in that, for

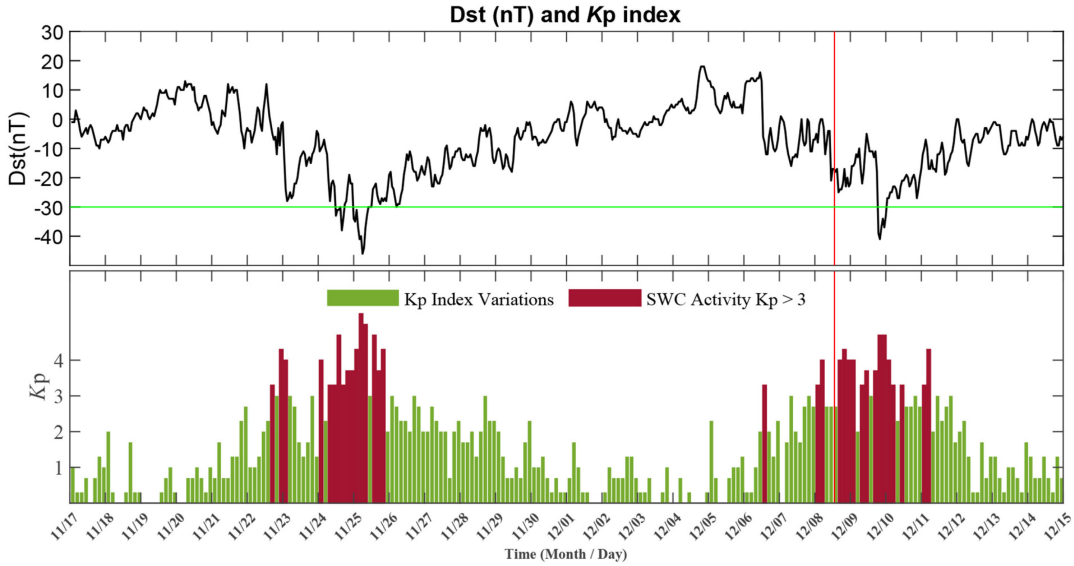

Fig. 11. Variations in the Dst and K_p geomagnetic and solar indices from November 17 to December 15, 2016.

traditional models, the performance of learning algorithms often relies on expert knowledge, whereas for deep learning models, more complex neural networks are used to learn high-level features of the data, without the need for expert feature classification. Although the results confirm that the ED-LSTME model can be used for short-term predictions, future research should focus more on the estimation of medium- and long-term TEC. In addition, storm time ionosphere predictions are usually associated with seasonal variations [51], which open up a new direction for subsequent research.

The comparison of earthquake TEC anomaly detection results shows that there are relatively large differences in detection based on the IQR method; in particular, the number of days with anomalies is significantly less than that detected by the ED-LSTME method, the detected anomalies are not sensitive to seismic activity, and there is no clear pattern of positive and negative anomalies. This may be related to the shortcomings of the IQR method, that is, the accuracy of the reference background value is low and the error limits are not reasonable, which is also the reason for the inconsistent results of the preseismic ionospheric disturbance anomalies studied by this method.

When geomagnetic activity is high during the days close to an earthquake, the observed ionospheric disturbances cannot be explained independently of solar-terrestrial events. However, in this study, only pre-earthquake TEC anomalies during geomagnetically relatively quiet periods were considered.

IV. Conclusion

We have proposed a new GNSS TEC-based detection model for earthquake ionospheric perturbation using a deep learning framework, the ED-LSTME model, and compared our approach with other traditional time-series prediction models for seismic TEC anomalies. Results show that the performance of the ED-LSTME model for predicting time-series TEC is significantly better than that of other traditional time-series prediction methods. In addition, to address the shortcomings of traditional seismic anomaly detection methods (e.g., the IQR method) in determining the upper and lower limits of anomalies, a more reasonable limit determination strategy was applied by using high-accuracy prediction values and reasonable upper and lower limits to achieve reasonable TEC anomaly detection. Finally, we analyzed pre-earthquake ionospheric TEC disturbance of the 2016 Xinjiang M_s 6.2 earthquake using the ED-LSTME model and drew the following conclusions.

1) On comparing the ED-LSTME model with five other benchmarking predictors on an independent test set, the proposed model achieved the best performance ($R^2 = 0.9105$ and RMSE $= 2.6759$), and demonstrated a 20% improvement in R^2 and 39.1% improvement in the RMSE over the ARIMA model. Overall, the proposed model achieved significant improvement in predicting TEC time series data.
2) Obvious ionospheric anomalies were detected 4–8 days and 1 day before the Xinjiang M_s 6.2 earthquake; these anomalies were not affected by external space weather such as solar or geomagnetic activity. The analysis of the spatial and temporal anomaly evolution of infrared OLR before and after the Xinjiang M_s 6.2 earthquake also confirms that these anomalies were caused by the earthquake. Therefore, it was shown that the pre-earthquake ionospheric anomalous disturbances were caused, to some extent, by the earthquake itself, suggesting that the use of pre-earthquake ionospheric disturbances may be a means of achieving short-term earthquake prediction.
3) The earliest ionospheric anomaly occurred 8 days before the Xinjiang M_s 6.2 earthquake; this anomaly continued until the earthquake occurred. Among other anomalies, the negative anomalies were mainly concentrated in the several days before the earthquake and occurred much earlier before the time of the earthquake, whereas the positive anomalies occurred closer to the time of the earthquake.

Moreover, the intensity of anomalies increased as the time of the earthquake approached.

Owing to it is the first case of detecting earthquake anomalies using the deep learning model ED-LSTME presented in this article, these findings require further investigation. In addition, owing to the complexity of earthquake mechanisms and the unclear physical mechanism of preseismic ionospheric disturbances, the use of ionospheric disturbances to predict short-term and imminent earthquakes needs further research. However, if verified, the results of this study can provide an important reference for more accurate predictions of earthquake occurrence.

REFERENCES

[1] M. B. Gokhberg, V. A. Morgounov, T. Yoshino, and I. Tomizawa, "Experimental measurement of electromagnetic emissions possibly related to earthquakes in Japan," *J. Geophys. Res.*, vol. 87, no. B9, pp. 7824–7828, 1982.

[2] M. Parrot *et al.*, "The magnetic field experiment IMSC and its data processing onboard DEMETER: Scientific objectives, description and first results," *Planet. Space Sci.*, vol. 54, no. 5, pp. 441–455, 2006, doi: 10.1016/j.pss.2005.10.015.

[3] S. A. Pulinets, T. B. Gaivoronska, A. Leyva Contreras, and L. Ciraolo, "Correlation analysis technique revealing ionospheric precursors of earthquakes," *Natural Hazards Earth Syst. Sci.*, vol. 4, no. 5/6, pp. 697–702, 2004, doi: 10.5194/nhess-4-697-2004.

[4] M. Hayakawa, R. Kawate, O. A. Molchanov, and K. Yumoto, "Results of ultra-low-frequency magnetic field measurements during the Guam earthquake of 8 August 1993," *Geophys. Res. Lett.*, vol. 23, no. 3, pp. 241–244, 1996, doi: 10.1029/95gl02863.

[5] J. Y. Liu, Y. I. Chen, Y. J. Chuo, and H. F. Tsai, "Variations of ionospheric total electron content during the Chi-Chi earthquake," *Geophys. Res. Lett.*, vol. 28, no. 7, pp. 1383–1386, 2001, doi: 10.1029/2000gl012511.

[6] J. Y. Liu, Y. I. Chen, C. H. Chen, and K. Hattori, "Temporal and spatial precursors in the ionospheric global positioning system (GPS) total electron content observed before the 26 December 2004 M9.3 Sumatra-Andaman earthquake," *J. Geophys. Res., Space Phys.*, vol. 115, no. A9, 2010, Art. no. 09312, doi: 10.1029/2010ja015313.

[7] X. Shen *et al.*, "The earthquake-related disturbances in ionosphere and project of the first China seismo-electromagnetic satellite," *Earthq. Sci.*, vol. 24, no. 6, pp. 639–650, 2011, doi: 10.1007/s11589-011-0824-0.

[8] X. Zhang, X. Shen, J. Liu, X. Ouyang, J. Qian, and S. Zhao, "Ionospheric perturbations of electron density before the Wenchuan earthquake," *Int. J. Remote Sens.*, vol. 31, no. 13, pp. 3559–3569, 2010, doi: 10.1080/01431161003727762.

[9] J. Y. Liu *et al.*, "Seismoionospheric GPS total electron content anomalies observed before the 12 May 2008 M_w7.9 Wenchuan earthquake," *J. Geophys. Res., Space Phys.*, vol. 114, no. A4, 2009, Art. no. A04320, doi: 10.1029/2008ja013698.

[10] J. Li, G. Meng, X. You, R. Zhang, H. Shi, and Y. Han, "Ionospheric total electron content disturbance associated with May 12, 2008, Wenchuan earthquake," *Geodesy Geodyn.*, vol. 6, no. 2, pp. 126–134, 2015, doi: 10.1016/j.geog.2015.01.003.

[11] K. Ryu *et al.*, "Suspected seismo-ionospheric coupling observed by satellite measurements and GPS TEC related to the M7.9 Wenchuan earthquake of 12 May 2008," *J. Geophys. Res., Space Phys.*, vol. 119, no. 12, pp. 10305–10323, 2014, doi: 10.1002/2014ja020613.

[12] L. He and K. Heki, "Three-dimensional distribution of ionospheric anomalies prior to three large earthquakes in Chile," *Geophys. Res. Lett.*, vol. 43, no. 14, pp. 7287–7293, 2016, doi: 10.1002/2016gl069863.

[13] K. Heki, "Ionospheric electron enhancement preceding the 2011 Tohoku-Oki earthquake," *Geophys. Res. Lett.*, vol. 38, no. 17, 2011, Art. no. L17312, doi: 10.1029/2011gl047908.

[14] J.-Y. Liu, C.-H. Chen, C.-H. Lin, H.-F. Tsai, C.-H. Chen, and M. Kamogawa, "Ionospheric disturbances triggered by the 11 March 2011 M9.0 Tohoku earthquake," *J. Geophys. Res., Space Phys.*, vol. 116, no. A6, 2011, Art. no. A06319, doi: 10.1029/2011ja016761.

[15] T. Iwata and K. Umeno, "Correlation analysis for preseismic total electron content anomalies around the 2011 Tohoku-Oki earthquake," *J. Geophys. Res., Space Phys.*, vol. 121, no. 9, pp. 8969–8984, 2016, doi: 10.1002/2016ja023036.

[16] M. Shah, A. C. Aibar, M. A. Tariq, J. Ahmed, and A. Ahmed, "Possible ionosphere and atmosphere precursory analysis related to $M_w > 6.0$ earthquakes in Japan," *Remote Sens. Environ.*, vol. 239, 2020, Art. no. 111620, doi: 10.1016/j.rse.2019.111620.

[17] H. Chen *et al.*, "Singular spectrum analysis of the total electron content changes prior to $M \geq 6.0$ earthquakes in the Chinese mainland during 1998–2013," *Front. Earth Sci.*, vol. 9, 2021, Art. no. 677163, doi: 10.3389/feart.2021.677163.

[18] F. Zhu and Y. Jiang, "Investigation of GIM-TEC disturbances before $M \geq 6.0$ inland earthquakes during 2003-2017," *Sci. Rep.*, vol. 10, no. 1, Oct. 2020, Art. no. 18038, doi: 10.1038/s41598-020-74995-w.

[19] M. Shah *et al.*, "Total electron content anomalies associated with earthquakes occurred during 1998–2019," *Acta Astronaut.*, vol. 175, pp. 268–276, 2020, doi: 10.1016/j.actaastro.2020.06.005.

[20] J. Y. Liu *et al.*, "Pre-earthquake ionospheric anomalies registered by continuous GPS TEC measurements," *Annales Geophysicae*, vol. 22, no. 5, pp. 1585–1593, 2004, doi: 10.5194/angeo-22-1585-2004.

[21] M. Saqib, E. Şentürk, S. A. Sahu, and M. A. Adil, "Ionospheric anomalies detection using autoregressive integrated moving average (ARIMA) model as an earthquake precursor," *Acta Geophys.*, vol. 69, pp. 1493–1507, 2021, doi: 10.1007/s11600-021-00616-3.

[22] Z. Xiao-Hong, R. Xiao-Dong, W. Fend-Bo, and C. Yu-Yang, "A new method for detection of pre-earthquake ionospheric anomalies," *Chin. J. Geophys.*, vol. 56, no. 2, pp. 441–449, 2013.

[23] M. Akhoondzadeh, "A MLP neural network as an investigator of TEC time series to detect seismo-ionospheric anomalies," *Adv. Space Res.*, vol. 51, no. 11, pp. 2048–2057, 2013, doi: 10.1016/j.asr.2013.01.012.

[24] M. Akhoondzadeh, "Investigation of GPS-TEC measurements using ANN method indicating seismo-ionospheric anomalies around the time of the Chile ($M_w = 8.2$) earthquake of 01 April 2014," *Adv. Space Res.*, vol. 54, no. 9, pp. 1768–1772, 2014, doi: 10.1016/j.asr.2014.07.013.

[25] M. Akhoondzadeh, "Decision tree, bagging and random forest methods detect TEC seismo-ionospheric anomalies around the time of the Chile, ($M_w = 8.8$) earthquake of 27 February 2010," *Adv. Space Res.*, vol. 57, no. 12, pp. 2464–2469, 2016, doi: 10.1016/j.asr.2016.03.035.

[26] M. Akhoondzadeh, "Support vector machines for TEC seismo-ionospheric anomalies detection," *Annales Geophysicae*, vol. 31, no. 2, pp. 173–186, 2013, doi: 10.5194/angeo-31-173-2013.

[27] J. N. Thomas, J. Huard, and F. Masci, "A statistical study of global ionospheric map total electron content changes prior to occurrences of $M \geq 6.0$ earthquakes during 2000-2014," *J. Geophys. Res., Space Phys.*, vol. 122, pp. 2151–2161, 2017, doi: 10.1002/2016ja023652.

[28] F. Masci, J. N. Thomas, and J. A. Secan, "On a reported effect in ionospheric TEC around the time of the 6 April 2009 L'Aquila earthquake," *Natural Hazards Earth Syst. Sci.*, vol. 17, no. 9, pp. 1461–1468, 2017, doi: 10.5194/nhess-17-1461-2017.

[29] H. Le, J. Y. Liu, and L. Liu, "A statistical analysis of ionospheric anomalies before 736 M6.0+ earthquakes during 2002-2010," *J. Geophys. Res., Space Phys.*, vol. 116, no. A2, 2011, Art. no. A02303, doi: 10.1029/2010ja015781.

[30] P. I. Nenovski, M. Pezzopane, L. Ciraolo, M. Vellante, U. Villante, and M. De Lauretis, "Local changes in the total electron content immediately before the 2009 Abruzzo earthquake," *Adv. Space Res.*, vol. 55, no. 1, pp. 243–258, 2015, doi: 10.1016/j.asr.2014.09.029.

[31] P. Xiong, D. Zhai, C. Long, H. Zhou, X. Zhang, and X. Shen, "Long short-term memory neural network for ionospheric total electron content forecasting over China," *Space Weather*, vol. 19, no. 4, 2021, Art. no. e2020SW002706, doi: 10.1029/2020sw002706.

[32] B. K. Choi, J. H. Cho, and S. J. Lee, "Estimation and analysis of GPS receiver differential code biases using KGN in Korean Peninsula," *Adv. Space Res.*, vol. 47, no. 9, pp. 1590–1599, 2011, doi: https://doi.org/10.1016/j.asr.2010.12.021.

[33] S. Moritz and T. Bartz-Beielstein, "ImputeTS: Time series missing value imputation in R," *R J.*, vol. 9, no. 1, pp. 207–218, 2017.

[34] E. Zivot and J. Wang, "Rolling analysis of time series," in *Modeling Financial Time Series With S-Plus*. New York, NY, USA: Springer, 2003, pp. 299–346.

[35] I. Sutskever, O. Vinyals, and Q. V. Le, "Sequence to sequence learning with neural networks," in *Proc. Adv. Neural Inf. Process. Syst.*, 2014, pp. 3104–3112.

[36] F. Chollet, *Deep Learning With Python*. Shelter Island, NY, USA: Manning Publ., 2017.

[37] Y. LeCun, Y. Bengio, and G. Hinton, "Deep learning," *Nature*, vol. 521, no. 7553, pp. 436–444, May 2015, doi: 10.1038/nature14539.

[38] L. Breiman, "Random forests," *Mach. Learn.*, vol. 45, no. 1, pp. 5–32, Oct. 2001, doi: 10.1023/a:1010933404324.
[39] U. Thissen, R. van Brakel, A. P. de Weijer, W. J. Melssen, and L. M. C. Buydens, "Using support vector machines for time series prediction," *Chemometrics Intell. Lab. Syst.*, vol. 69, no. 1/2, pp. 35–49, 2003, doi: 10.1016/s0169-7439(03)00111-4.
[40] P. H. Swain and H. Hauska, "The decision tree classifier: Design and potential," *IEEE Trans. Geosci. Electron.*, vol. GE-15, no. 3, pp. 142–147, Jul. 1977.
[41] S. Makridakis and M. Hibon, "ARMA models and the Box–Jenkins methodology," *J. Forecasting*, vol. 16, no. 3, pp. 147–163, 1997.
[42] S. Sahu, R. Trivedi, R. K. Choudhary, A. Jain, and S. Jain, "Prediction of total electron content (TEC) using neural network over anomaly crest region Bhopal," *Adv. Space Res.*, vol. 68, no. 7, pp. 2919–2929, 2021, doi: 10.1016/j.asr.2021.05.027.
[43] A. A. Akyol, O. Arikan, and F. Arikan, "A machine learning-based detection of earthquake precursors using ionospheric data," *Radio Sci.*, vol. 55, no. 11, Nov. 2020, Art. no. e2019RS006931, doi: 10.1029/2019rs006931.
[44] J. Y. Liu, Y. I. Chen, S. A. Pulinets, Y. B. Tsai, and Y. J. Chuo, "Seismo-ionospheric signatures prior to M≥6.0 Taiwan earthquakes," *Geophys. Res. Lett.*, vol. 27, no. 19, pp. 3113–3116, 2000, doi: 10.1029/2000gl011395.
[45] K. E. Taylor, "Summarizing multiple aspects of model performance in a single diagram," *J. Geophys. Res., Atmos.*, vol. 106, no. D7, pp. 7183–7192, 2001, doi: 10.1029/2000jd900719.
[46] R. Song, X. Zhang, C. Zhou, J. Liu, and J. He, "Predicting TEC in China based on the neural networks optimized by genetic algorithm," *Adv. Space Res.*, vol. 62, no. 4, pp. 745–759, 2018, doi: 10.1016/j.asr.2018.03.043.
[47] V. Tramutoli, V. Cuomo, C. Filizzola, N. Pergola, and C. Pietrapertosa, "Assessing the potential of thermal infrared satellite surveys for monitoring seismically active areas: The case of Kocaeli (İzmit) earthquake, August 17, 1999," *Remote Sens. Environ.*, vol. 96, no. 3/4, pp. 409–426, 2005.
[48] N. Genzano, C. Filizzola, K. Hattori, N. Pergola, and V. Tramutoli, "Statistical correlation analysis between thermal infrared anomalies observed from MTSATs and large earthquakes occurred in Japan (2005–2015)," *J. Geophys. Res., Solid Earth*, vol. 126, no. 2, 2021, Art. no. e2020JB020108, doi: 10.1029/2020jb020108.
[49] P. Xiong and X. Shen, "Outgoing longwave radiation anomalies analysis associated with different types of seismic activity," *Adv. Space Res.*, vol. 59, no. 5, pp. 1408–1415, Mar. 2017, doi: 10.1016/j.asr.2016.12.011.
[50] D. Tien Bui *et al.*, "A novel deep learning neural network approach for predicting flash flood susceptibility: A case study at a high frequency tropical storm area," *Sci. Total Environ.*, vol. 701, Jan. 2020, Art. no. 134413, doi: 10.1016/j.scitotenv.2019.134413.
[51] R. Tang, F. Zeng, Z. Chen, J.-S. Wang, C.-M. Huang, and Z. Wu, "The comparison of predicting storm-time ionospheric TEC by three methods: ARIMA, LSTM, and Seq2Seq," *Atmosphere*, vol. 11, no. 4, 2020, Art. no. 316, doi: 10.3390/atmos11040316.

Pan Xiong received the B.Eng. degree in science and technology of remote sensing from Wuhan University, Wuhan, China, in 2006, and the Ph.D. degree in cartography and geography information system from the Chinese Academy of Sciences, Beijing, China, in 2014.

He is currently an Associate Professor with the Institute of Earthquake Forecasting, China Earthquake Administration, Beijing, China. His current research focuses on the development of data mining/machine learning algorithms that enable a system to better understand and interpret precursory anomalies before main earthquake from satellite data. His research has been or is supported by several projects including the National Key Research and Development Program of China and the National Key Technology R&D Program of China.

Cheng Long (Senior Member, IEEE) received the B.Eng. degree from the South China University of Technology, Guangzhou, China, in 2010, and the Ph.D. degree from the Hong Kong University of Science and Technology, Hong Kong, in 2015, both in computer science and technology.

He is currently an Assistant Professor with the School of Computer Science and Engineering, Nanyang Technological University, Singapore. From 2016 to 2018, he was a Lecturer with Queen's University Belfast, Belfast, U.K. His research interests include data management, data mining, and big data analytics.

Dr. Long was a Program Committee Member/Referee for several top data management and data mining conferences/journals such as *ACM Transactions on Database Systems*, *VLDB J*, IEEE TRANSACTIONS ON KNOWLEDGE AND DATA ENGINEERING, IEEE International Conference on Data Mining, Conference on Information and Knowledge Management, etc.

Huiyu Zhou received the B.Eng. degree in radio technology from the Huazhong University of Science and Technology, Wuhan, China, in 1990, the M.Sc. degree in biomedical engineering from the University of Dundee, Dundee, U.K., and the Ph.D. degree in computer vision from Heriot-Watt University, Edinburgh, U.K., in 2006.

He is currently a Professor with the School of Computing and Mathematical Sciences, University of Leicester, Leicester, U.K. He has authored more than 400 peer-reviewed papers in his research field. His research work has been or is being supported by U.K. EPSRC, MRC, EU, Royal Society, Leverhulme Trust, Puffin Trust, Invest NI, and industry.

Xuemin Zhang received the B.Sc. degree in geophysics from Yunnan University, Kunming, China, in 1991, the M.Sc. degree in solid state geophysics from the University of Science and Technology of China, Hefei, China, in 2001, and the Ph.D. degree in earth exploration and information technology from the China University of Geosciences, Wuhan, China, in 2005.

She is currently a Professor in seismo-electromagnetics with the Institute of Earthquake Forecasting, China Earthquake Administration, Beijing, China. She is the Deputy Chairman of the Committee of Seismo-Electromagnetics, Seismological Society of China. She has authored/coauthored more than 100 journal papers. Her research interests include seismo-electromagnetics, ionospheric physics, radio wave propagation and ionospheric heating, and machine learning, with more than 20 research projects supported by the NSFC, MOST, and other funding agencies.

Dr. Zhang is an Associate Editor-in-Chief for the *Journal of Earthquake*.

Xuhui Shen received the Ph.D. degree in tectonic geology from the Institute of Geology, China Earthquake Administration, Beijing, China, in 1996.

He is currently a Professor with the National Institute of Natural Hazards, Ministry of Emergency Management of China, Beijing, China. He is also the Chief Scientist and Deputy Chief Designer of the China electromagnetic monitoring test satellite project. He is mainly engaged in the research works of seismotectonics and new tectonics, satellite seismic applications, and geophysical remote sensing techniques for a long time.